catalysts

MDPI

Article

Peptide-Functionalized Gold Nanoparticles as Organocatalysts for Asymmetric Aldol Reactions

Thabo Peme [1,*], Dean Brady [1], Ndivhuwo P. Shumbula [1], Khanani Machumele [1], Nosipho Moloto [1], Taryn Adams [2] and Maya M. Makatini [1,*]

[1] Molecular Sciences Institute, School of Chemistry, University of the Witwatersrand, PO WITS, Johannesburg 2050, South Africa; dean.brady@wits.ac.za (D.B.); ndivhuwos@mintek.co.za (N.P.S.); khanza.mach@gmail.com (K.M.); nosipho.moloto@wits.ac.za (N.M.)

[2] Protein Structure-Function Research Unit, School of Molecular and Cell Biology, Faculty of Sciences, University of Witwatersrand, PO WITS, Johannesburg 2050, South Africa; taryn.adams16@gmail.com

* Correspondence: thabopeme@gmail.com (T.P.); maya.makatini@wits.ac.za (M.M.M.)

Abstract: The use of high catalyst loading is required for most of the organocatalyzed asymmetric aldol reactions in organic synthesis, and this often presents challenges during purification and difficulties in catalyst recovery from the reaction mixture. The immobilization of the catalyst onto gold nanoparticles (AuNPs) can change the structural conformations of the catalyst, thereby improving its catalytic activity and reusability. Herein we report on the synthesis of aldolase mimetic peptide coupled to gold nanoparticles (AuNPs) as efficient organocatalysts for asymmetric aldol reaction. AuNPs were synthesized using the Turkevich method. The conjugation of the peptide to AuNPs was characterized using surface plasmon resonance (SPR), Raman and X-ray photoelectron spectroscopy, and transmission electron microscopy (TEM) was used for particle size determination. The produced nanoparticles, whose sizes depended on the reduction method, were quasi-spherical with a relatively narrow size distribution. The peptide–AuNP conjugates were evaluated for aldol reaction catalytic activity between carbonyls *p*-nitrobenzaldehyde and cyclohexanone. The products were obtained with good yields (up to 85%) and enantioselectivity (up to 94%). The influence of organic solvents, pH and buffer solutions was also investigated. The results showed that the buffer solutions regulated the colloidal stability of AuNPs, resulting in a significant enhancement in the catalytic rate of the peptide–AuNP conjugate.

Keywords: peptide; nanoparticles; aldol reaction; catalytic activity

Citation: Peme, T.; Brady, D.; Shumbula, N.P.; Machumele, K.; Moloto, N.; Adams, T.; Makatini, M.M. Peptide-Functionalized Gold Nanoparticles as Organocatalysts for Asymmetric Aldol Reactions. *Catalysts* **2024**, *14*, 826. https://doi.org/10.3390/catal14110826

Academic Editor: Werner Oberhauser

Received: 6 May 2024
Revised: 3 November 2024
Accepted: 5 November 2024
Published: 16 November 2024

1. Introduction

The use of organic compounds as asymmetric catalysts complements the conventional use of organometallic and biocatalytic approaches in asymmetric catalysis. Organocatalysis has recently gained considerable attention in the synthesis of chiral molecules and has been designated the third general approach to the catalytic production of enantiopure compounds [1–3]. However, most asymmetric reactions in organic synthesis require relatively high catalyst loading, and this often presents challenges such as the purification of products and difficulties in the separation of the catalyst from the reaction mixture [4]. Due to the rise in demand for optically pure compounds, a lot of work has been done to develop efficient stereoselective methodologies in organocatalysis [5–7]. The immobilization of asymmetric catalysts onto solid carriers or polymers has shown some impressive results in terms of reusability and product isolation [8]. There are several techniques used in the immobilization of catalysts on solid supports [9] or ionic liquids [10], reported in the literature for providing sustainable organocatalytic systems. Nanoparticles (NPs) have gained significant attention in recent years, with wide applications in sensing, drug discovery, novel therapy, catalysis, and control of protein structure and activity [11–14]. In particular, gold nanoparticles (AuNPs), because of their size- and shape-dependent

properties and ease of synthesis and surface functionalization, have become increasingly popular for the development of supported catalysts [12,13,15]. In addition, AuNPs can be simply functionalized using biomolecules possessing amines or thiols and phosphine moieties [13]. Cysteine is most likely to bind to AuNPs through its thiol (–SH) group, and this bond is formed by a ligand exchange reaction between cysteine and citrate-capped gold nanoparticles [16,17]. To date, most of the work reported in the literature involves the immobilization of enzymes onto gold nanostructures in attempts to improve enzymatic activity and stability, change substrate specificity [18,19], as well as create enzyme mimics [20,21]. Studies involving the conjugation of peptides to AuNPs have been focused on the detection of heavy metals [22,23] and on biomedical applications for drug delivery and cellular uptake [11,24]. However, few studies have been reported on peptide–AuNPs as catalysts for organic synthetic reactions [20,25,26]. Previous work has focused on proline and its derivatives [10,27,28]. In this study, peptide–AuNP conjugates are utilized as organocatalysts for aldol reactions. The aldol reaction is one of the most useful C-C bond-forming reactions in organic synthesis [5]. Most of the traditional catalysts reported in the literature for the aldol reaction have a few drawbacks, such as the use of excess amounts of hazardous solvents and high catalyst loading, which hinders progress toward efficient, environmentally friendly, sustainable catalysts. Among several organocatalysts reported for the aldol reaction, peptides have received considerable attention in recent years [29,30]. The use of peptides as biocatalysts has advantages, such as ease of synthesis and purification, and their structural and functional diversity provides multiple sites for modification, which can be easily attained by changing the sequences of amino acid residues [31–33]. Although significant improvements have been made in the design of peptide catalysts incorporating a secondary structural framework, there are still some limitations in catalyst reactivity. Peptides functionalized onto the surface of gold nanoparticles have been shown to form new functional nanoparticles with enzyme-like structures and properties [20,21]. The conjugation of polypeptides to NPs has the potential to influence both function and structure, and this effect depends on the sequence of the peptide [34]. Recently, we reported on mimetic peptides modelled on the catalytically active site of the fructose-1,6-bisphosphate aldolase (FBPA) enzyme as a catalyst for aldol reactions [35]. The peptide-catalyzed aldol reaction between aromatic aldehydes and cyclohexanone was demonstrated with notable catalytic activity and selectivity. The findings further proved that a large amount of catalyst was required for the rapid conversion of the substrate and to improve the yield (Scheme 1). Herein, we report on the catalytic activity and stability of peptide-functionalized gold nanoparticles in an aldol reaction.

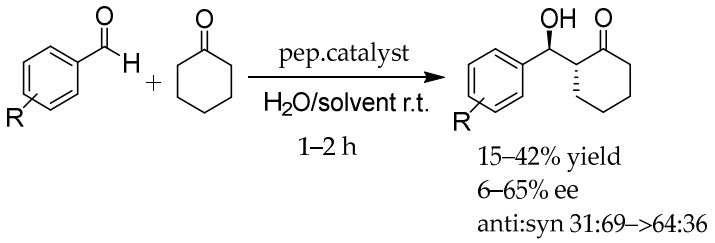

Scheme 1. Aldol reactions catalyzed by FBPA peptide mimics [35].

2. Results and Discussion

2.1. Rational Design of the Peptide

The peptide TP_ADLys was designed and synthesized as previously reported [35]. The peptide catalyst sequence consists of cysteine residues at each terminus [C(-COOH) and N(-NH_2)] of the peptides (Figure 1).

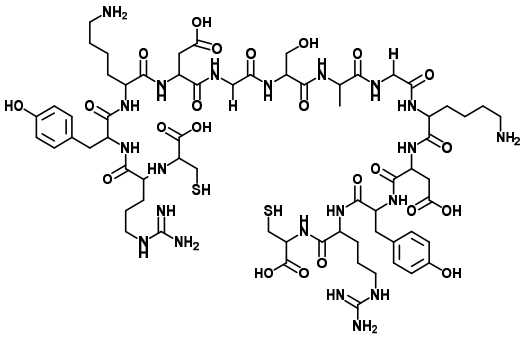

Figure 1. Schematic representation of the peptide.

Amino acids are known to interact with the gold surface specifically through their side chains; therefore, the two cysteines were incorporated as the side chain sulphur atoms have a high affinity for the AuNPs' surface [16], which allows efficient conjugation. The catalyst also possesses amino acids with hydrophobic side chains, [Alanine (A) and glycine (G)], which are known to promote self-assembly and stability of the peptide in water [36]. These hydrophobic interactions, together with hydrogen bonding formed between the peptide's backbone amides and the NPs, are thought to provide efficient packing of the molecules onto the NPs' surface. In addition, the NPs can reduce the peptide's mobility, thus promoting stability [36,37]. Lysine residues form enamine intermediates during aldol catalytic reactions and are also believed to participate in coordination bonding with AuNPs through the amine functional group [38]. The optimal conditions (such as the solvent medium and solution pH) that allow sufficient coverage of the surface while ensuring the stability of the nanoparticles during catalytic reaction were also taken into consideration.

2.2. Synthesis of Gold Nanoparticles and Peptide Functionalization

Gold nanoparticles were synthesized by the reduction of hydrogen tetrachloroaurate ($HAuCl_4$) with trisodium citrate. The reduction of gold chloride (III) using citrate has a few advantages, such as the fact that the citrate can be readily displaced, allowing for easy conjugation of the particles. The biomolecules of peptides or proteins containing thiols, amine and phosphine moieties can be used for functionalization since the synthesis is performed in an aqueous medium [39,40]. To obtain different sizes of AuNPs, different volumes of 0.04 M citrate solution (20, 30 and 50 mL) were added to the aqueous solution of $HAuCl_4$ (250 mL, 1 mM). This also allowed for the efficiency of the reductant, which mostly depends on its concentration [41]. To investigate the optical properties of both the gold colloidal solutions and peptide–AuNP conjugates, both solutions were analysed using UV–vis spectrophotometry. The absorption profile obtained for citrate-capped AuNPs revealed a damped localized plasmon resonance (LSPR) band peaking around 518, 520 and 523 nm for AuNP-20, AuNP-30 and AuNP-50, respectively (AuNPS-20 denotes labelling for AuNPs prepared with 20, 30 or 50 mL citrate; AuNPs-20P denotes labelling for peptide coupled to AuNPs prepared with 20 mL citrate), thus confirming the formation of quasi-spherical AuNPs (Figure 2). This observation illustrates the effect of collective oscillations of conducting electrons when interacting with electromagnetic radiation [42]. Furthermore, the magnitude of the shift differs with both the refractive index of the adsorbed layer and its thickness [43,44]. The gradual increase in shift of the AuNPs as the citrate volume increased further demonstrates the dependence of LSPR on the size of the nanoparticle. The literature suggests that a higher citrate ratio affords smaller nanoparticles [45].

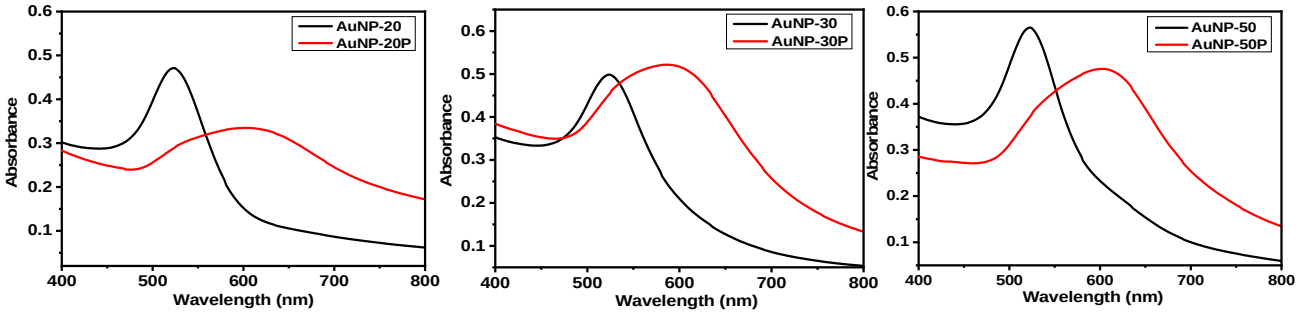

Figure 2. UV–vis absorption spectra showing the LSPR band for citrate-capped AuNPs (black line) and peptide–AuNPs (red line).

The peptide was functionalized by incubating the obtained particle sizes in different peptide concentrations in Milli-Q water for 3–12 h, followed by successive washes to ensure complete coupling of the peptides and to reduce the concentration of nonconjugated peptide [46]. Furthermore, a broader absorbance shoulder was seen with a strong plasmon band at 605, 600 and 595 nm for AuNP-20P, AuNP-30P and AuNP-50P, respectively, when the particles were introduced to the peptide solution. The large LSPR shift observed suggests a strong interparticle interaction, confirming the conjugation of the peptide to AuNPs. Additionally, this shift is due to the change in the refractive index in the vicinity of the particle surface during the immobilization of the peptide [47]. The broader surface plasmon also indicates the change in the dielectric constant, which is attributed to the agglomeration of the nanoparticles. To further understand the specific interaction between the gold nanoparticles and the peptide, and the arrangement within the nanoparticles, transmission electron microscopy (TEM) analyses were carried out (Figure 3). The images of the citrate-capped NPs shown in Figure 3a–c reveal roughly quasi-spherical particles with a fairly narrow size distribution. Furthermore, the results also indicate that the particles are polycrystalline. When the gold nanoparticles were functionalized with the peptides, the particles were fairly dispersed due to the ionic nature of the peptide surface, causing a slight electrostatic repulsion of the individual particles (Figure 3d–f).

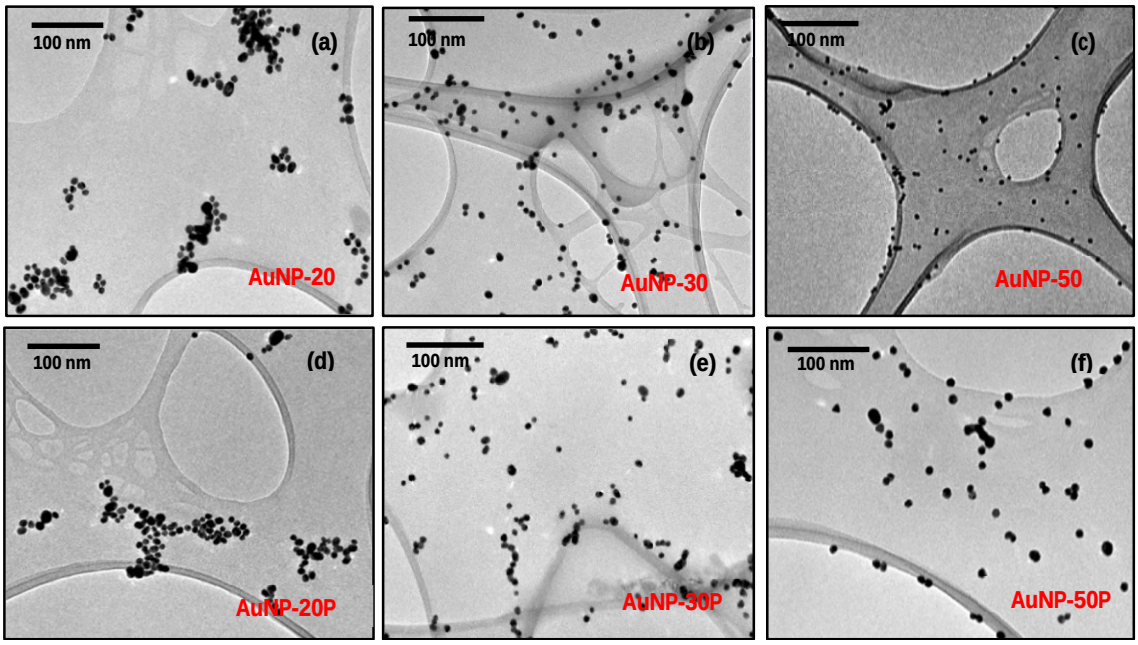

Figure 3. TEM images of citrate–AuNPs and peptide–AuNPs: (**a**) AuNP-20, (**b**) AuNP-30, (**c**) AuNP-30, (**d**) AuNP-20P, (**e**) AuNP-30P and (**f**) AuNP-50P.

The obtained TEM images were utilized to measure nanoparticle size distribution and the average diameter using ImageJ software (Imagej 2006, v.1.4.3.67) [48]. The histograms, which provide a visual representation of the average size of the particles, reveal an average diameter ranging from 12 to 16 nm (Figure 4). A relationship involving the surface-to-volume ratio can be seen, as there is a slight decrease in the average size as the citrate ratio increases. This effect can be attributed to a slight agglomeration of nanoparticles (Figure 4) prior to functionalization, which can result in a slow substitution reaction of the citrate by the peptide [49]. One of the contributing factors leading to aggregation is the high surface area-to-volume ratio, which leads to thermodynamically unstable small Au clusters, as reported in the literature [50,51]. Moreover, other studies postulate that aggregation is due to van der Waals forces and the tendency of Au(III) complexes to attract metallic Au surfaces [52,53]. In parallel, when the peptide was conjugated to the nanoparticle, there was a decrease in average particle diameter from 13.53 ± 3.5 to 11.9 ± 2.47. The observed results were consistent with those reported in previous studies [38]. This observation suggests that the binding affinity plays a vital role in governing the interactions between the peptide and the growing particle size [54]. The mechanism can also be explained in terms of the effect called 'bridging flocculation', which describes the binding of a peptide molecule to more than one particle at a time [38]. The chelate formed between the sulfhydryl group of the cysteine residue of the peptide and Au^{3+} can also restrict the growth of AuNPs by prohibiting further nucleation of the free remaining gold ions [41,55].

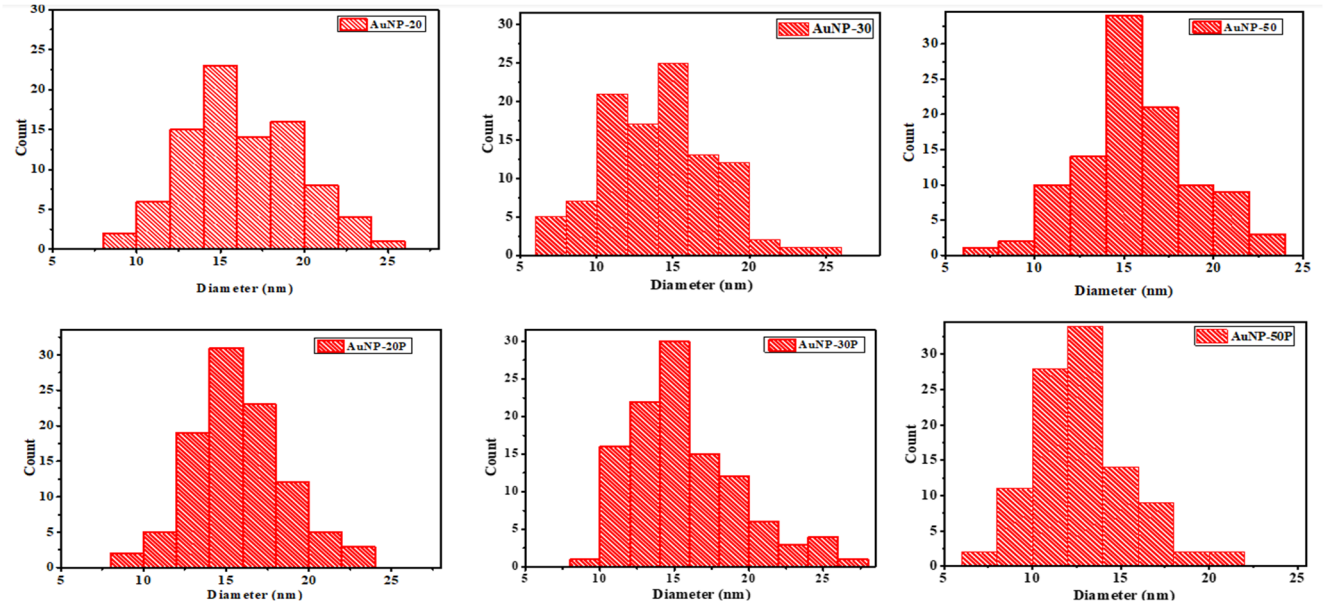

Figure 4. Particle distribution histogram of citrate-capped AuNPs and peptide–AuNPs.

2.3. Characterization Using Raman and X-Ray Photoelectron Spectroscopy

The survey spectrum of citrate-capped AuNPs (Figure 5) shows a peak attributed to AuNPs, along with peaks for carbon (C) and oxygen (O) (the C1s high-resolution spectrum is shown in Figure S28), which are associated with the citrate ligands on the surface of the gold. The presence of sodium (as shown in the high-resolution spectrum in Figure S28) suggests that free sodium citrate molecules are also present. In the survey spectrum of peptide–AuNPs (Figure 5), the appearance of the N1s peak (high-resolution spectrum shown in Figure S28) indicates ligand exchange, whereby the citrate molecules have been replaced by the peptide. The prominence of the Au4f peak suggests the complete removal of the sodium citrate capping agent, with the AuNPs now stabilized by the peptide. Consequently, in this case, the C1s (high-resolution spectrum in Figure S28) and O1s peaks can be attributed to the peptide.

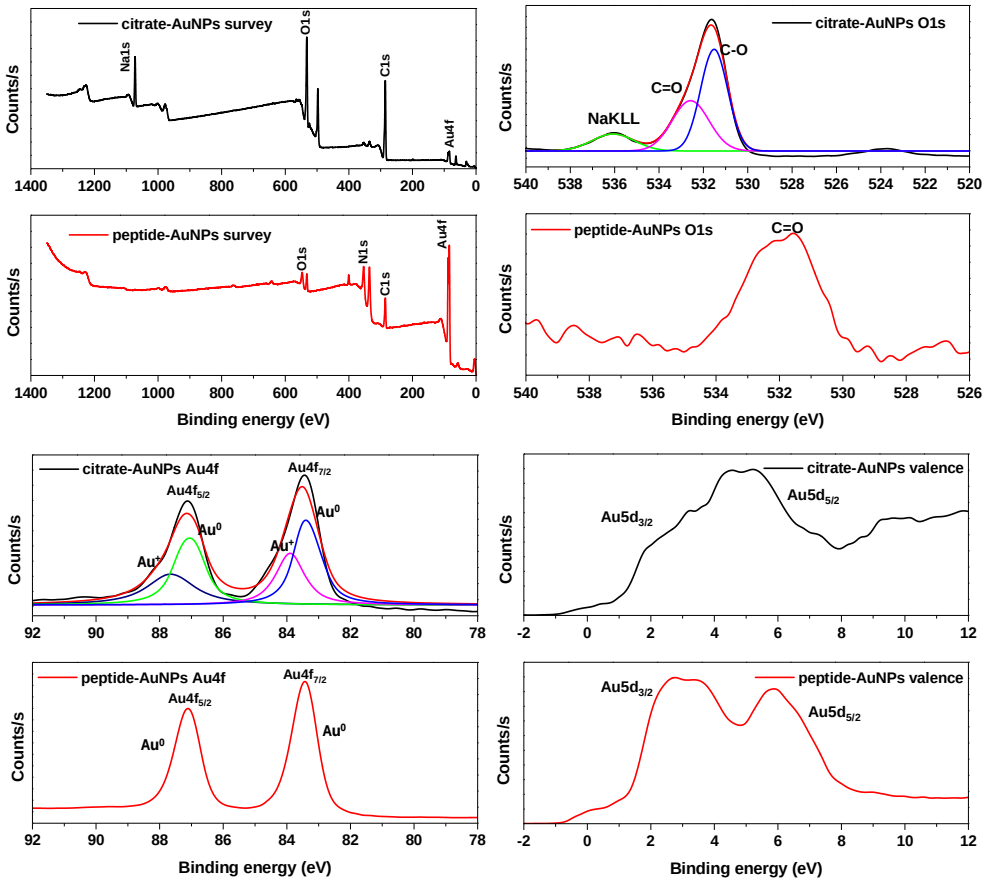

Figure 5. X-ray photoelectron survey and high-resolution (O1s, Au4f and valence) spectra of citrate-capped AuNPs (black line) and peptide–AuNPs (red line).

To further analyse the samples, high-resolution core-level spectra of both citrate-capped AuNPs and peptide–AuNPs were examined (Figure 5). The O1s spectrum of citrate–AuNPs shows the presence of sodium citrate functional groups, while the absence of sodium in the O1s spectrum of peptide–AuNPs confirms the ligand exchange (Scheme 2). The Au4f high-resolution spectrum of citrate–AuNPs is characterized by two pairs of peaks due to the 4f7/2 and 4f5/2 spin–orbit coupling. The first and most significant pair (83.3 eV and 87.1 eV) is attributed to elemental gold (Au^0), while the other pair (84.5 eV and 88.2 eV) is associated with oxidized gold. This oxidation may result from exposure to oxygen [56] or from the high surface area-to-volume ratio of the nanoparticles, which makes them more reactive. Surface atoms can interact with their environment, leading to oxidation or charge transfer, which can produce Au^+ species [57]. In some cases, Au^+ can form as a charge compensation mechanism, especially in the presence of defects [58]. The disappearance of Au^+ peaks in the XPS spectrum after conjugating the peptide to AuNPs may be attributed to several factors. First, the peptide may act as a reducing agent, converting Au^+ back to its elemental state (Au^0) [59]. Additionally, the conjugation may passivate the nanoparticle surface, preventing further oxidation and stabilising Au^0 [60].

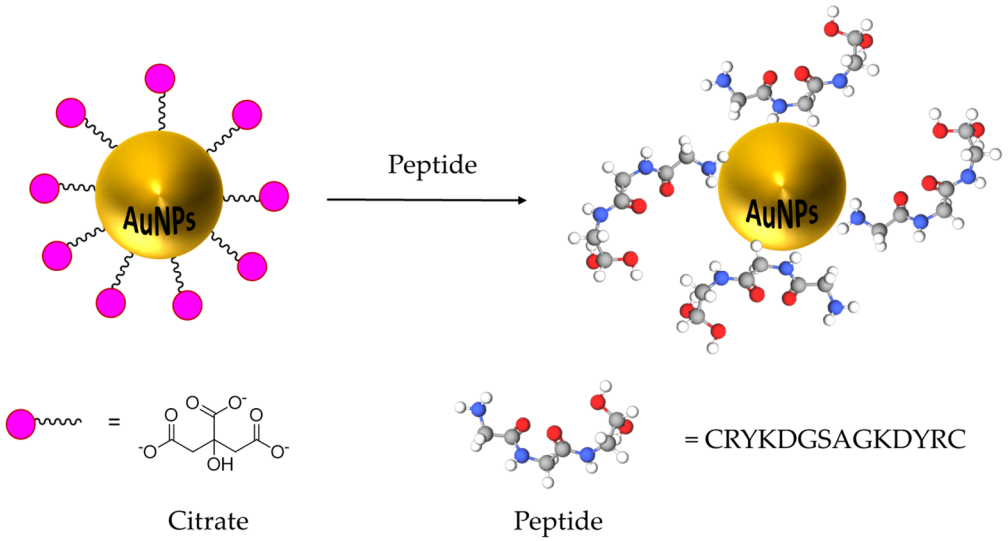

Scheme 2. Schematic representation of peptide–AuNPs synthesized from citrate-capped gold nanoparticles.

Changes in the electronic environment due to peptide binding can also favour Au^0 over Au^+ [61]. Furthermore, peptide-induced aggregation of the nanoparticles may enhance their stability, reducing the likelihood of oxidized species [62]. The valence spectrum of AuNPs reveals critical information about their electronic structure and oxidation states. Typically, a characteristic peak associated with metallic gold (Au^0) is observed around 2.5 to 4 eV binding energy, reflecting contributions from the 5d and 6s orbitals. Oxidized states, such as Au^+ or Au^{3+}, may introduce new features or shifts in peak positions, indicating the formation of new electronic states. The unique electronic structure of nanoparticles, influenced by their high surface area-to-volume ratio and potential interactions with surface ligands or biomolecules, can also alter the valence band profile. These insights help to understand the reactivity and stability of gold nanoparticles in various applications [59,61,62]. The valence spectrum of citrate-stabilized AuNPs is primarily characterized by contributions from the gold 5d orbitals. This spectrum features a doublet of peaks with weighted centres at 5.87 eV and 3.02 eV. Both peaks exhibit fine structure, which is attributed to the overlap of filled 5d orbitals from neighbouring gold atoms in the lattice. The shift in the doublet peaks to 4.83 eV and 2.24 eV after exchanging citrate for a peptide suggests a significant change in the electronic environment of the AuNPs. This lower energy shift indicates alterations in the electronic structure, possibly due to increased electron density in the 5d orbitals and modified bonding interactions with the peptide ligands. Such changes may reflect an altered ligand field around the gold atoms, influencing their reactivity and stability. These shifts highlight the peptide's impact on the surface chemistry and electronic properties of the AuNPs, which could affect their performance in various applications.

To further confirm the conjugation of the peptides to the AuNPs, Raman spectroscopy was conducted (Figure S29). The absence of peaks in the Raman spectrum of a peptide when analysed with a 532 nm laser can be attributed to the inherently weak Raman scattering of peptides, which often results from their simple molecular structures. However, upon conjugation to gold nanoparticles (AuNPs), the Raman signals are significantly enhanced due to Surface-Enhanced Raman Scattering (SERS). This enhancement occurs because the localized surface plasmon resonance (LSPR) of the AuNPs amplifies the Raman scattering of the nearby peptides, allowing for clearer peaks in the spectrum [63]. Additionally, the conjugation may alter the molecular orientation and environment of the peptide, leading to new peaks, and the aggregation of peptides around the AuNPs further increases the density of the analyte near the metal surface [64].

2.4. Aldol Reaction Catalyzed by Peptide–AuNPs

The catalytic activity of the peptide-supported catalyst was then demonstrated in an asymmetric aldol reaction. The use of water 'as a solvent' or co-solvent in chemical reactions has attracted a lot of attention due to its potential and advantages such as safety, low cost, availability, efficiency, and reactivity when compared to common organic solvents, and lastly, its impact on the environment that avoids issues of pollution which are inherent with common organic solvents [65]. However, it is worth noting that the use of an excess amount of water in reactions often results in poor mass transfer [66], while conversely, a small addition of water can accelerate the reaction and improve selectivity [5,67]. The activity of the functionalized peptide–AuNPs was investigated using the benchmark reaction between *p*-nitrobenzaldehyde and cyclohexanone and the results are summarized in (Table 1).

Table 1. Aldol reactions between *p*-nitrobenzaldehyde and cyclohexanone catalyzed by peptide–AuNPs [a].

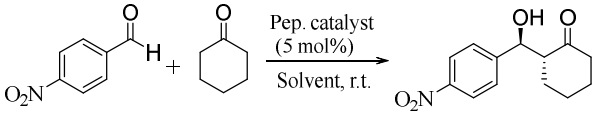

Entry	Particle Size (nm)	Solvent	Peptide.Cat (mol%)	Time (h)	Yield (%) [b]	ee (%) [c]	dr (Anti:Syn) [d]
1	16	Ketone [a]	6	96			
2	15		4	96	Trace	–	–
3			6	96	Trace	–	–
4	12		4	96	Trace	–	–
5			6	96	15	26	26:74
6 [f]	-	Ketone [e]	4	48	15	5	49:51
7 [f]	-		8	48	40	6	59:41
8	16	DMSO [g]	6	96	Trace	–	–
9	15		4	96	Trace	–	–
10			6	96	16	51	62:38
11	12		4	96	15	48	46:54
12			6	96	17	39	44:56
13 [f]	-	DMSO [h]	8	72	20	6	58:42
14 [f]	-	DMSO/H_2O [i]	8	72	27	31	64:36
15	16	Buffer [j]	6	72	21	76	57:43
16	15		6	72	39	94	59:41
17	12		6	72	44	78	56:44
18 [f]	-	Buffer [k]	8	72	38	80	57:43

[a] The reaction was performed using *p*-nitrobenzaldehyde (0.157 mmol, 24 mg) and 0.5 mL of cyclohexanone/AuNPs solution. [b] Isolated yield. [c] ee values were determined by chiral-phase HPLC analysis. [d] Determined by ^{1}H NMR analysis of the crude product. [e] The reaction was performed in ketone (cyclohexanone)/water 20:1 (*v*/*v*). [f] Results previously reported [35]. [g] The reaction was performed using cyclohexanone (0.628 mmol, 70 µL) in 1 mL DMSO/AuNPs solution. [h] The reaction was performed using cyclohexanone (0.628 mmol, 70 µL) in 0.75 mL plain DMSO. [i] The reaction was performed in 0.75 mL (0.51 mL DMSO and 0.24 mL water). [j] Reaction was performed using 0.50 mL phosphate buffer solution in AuNP solution (1:1) at r.t. [k] The reaction was performed in a phosphate buffer (0.5 mL).

The reactions were monitored using TLC (thin-layer chromatography). In order to assist the solubility of the substrates and optimize conditions for the conversion of the substrate, the reactions were performed in 50% ketone, 30% DMSO and buffered solutions. The solvent plays a vital role in influencing the reaction kinetics and the evolution of the transition state [68]. The use of a ketone (cyclohexanone) as a solvent has been shown to promote aldol reactions more efficiently than organic solvents [35,69]. DMSO was chosen because it is commonly used in aldol reaction studies and has previously shown good results [35,65,70]. In order to obtain the optimum reaction conditions with enhanced

catalytic activity, various peptide–AuNP sizes were investigated. When the reactions were performed in a cyclohexanone/AuNPs system for both 16 and 15 nm sizes, only a trace amount of the product was observed (Table 1, entries 1–4). This outcome could be attributed to the low solubility of cyclohexanone in aqueous AuNP solution, creating a biphasic system, thereby compromising the catalytic efficiency [71]. This phenomenon also explains the difference observed in the increase in catalytic performance using a free peptide (entries 6 and 7). There were highly promising results when the reactions were performed with 12 nm (entry 5) in cyclohexanone (with 15% yield). When nanoparticle size stability experiments were performed (see Figure S27), the TEM images revealed that AuNPs with bigger particle sizes (15 and 16 nm) agglomerate faster than the smaller particle sizes (12 nm). The stability of the AuNP solution was also monitored by the colour change and UV absorbance spectra. Therefore, the observed activity in entry 5 could be associated with the dependence of surface coverage of AuNPs on peptide concentration, which is in agreement with previously reported work [19,72]. Moreover, when the reactions were performed in aqueous DMSO using 16 nm AuNPs (entries 8 and 9), only a trace amount of product was observed, thus indicating the inactivity of large particle sizes. Comparatively, there was considerable improvement in yields (up to 17%) when nanoparticles with smaller sizes were used (entries 10–12). The slow reaction rate is reported to be due to poor dispersal of the catalyst and also the aggregation of the catalyst in DMSO [5]. These findings further demonstrate that increasing the catalyst concentration and modifying the solvent system can lead to an improvement in catalytic efficiency. In support of this observation, the literature reports that factors such as pH solution, ionic strength and composition of buffers can influence the interaction between peptide molecules and gold nanoparticles [73,74]. The biocatalytic performance for the AuNP–peptide-catalyzed aldol reactions was further evaluated in a buffered solution (entries 15–17). In selecting the initial pH for the reaction medium, the isoelectric point (pI) of the peptide, which is known to influence the aggregation or stability of the particles [38,75], was taken into consideration. At neutral pH, TP_ADLys peptide has a charge of 2.9, and the calculated isoelectric point (pI) is 9.6. At pH greater than 8, the reaction may become base-catalyzed [76], and in addition, studies report that if the pH is closer to the pI value, the material may show limited stability [77]; therefore, the reactions were performed at pH 7. There was a significant improvement in both the yields (up to 44%), enantiomeric excess (ee) (up to 80%) and a moderate improvement in the diastereoselectivity (dr) (59:41) for the aldol reactions in buffered solutions. The satisfactory results obtained in the buffered system promoted a search for an optimal buffering condition with the goal of improving the catalytic efficiency of the aldol reaction while still ensuring colloidal stability for AuNPs is maintained. The reactions were performed in citrate, phosphate and Tris-buffer at pH 5.8, 6.5 and 7.0, and the results are presented in Table 2 below using 12 nm AuNPs.

The choice of buffers and pHs used for the reactions was informed by their aldol reaction catalytic efficiency and selectivity, as previously reported in the literature [76,78]. In addition, the selection of buffers was based on the ability to allow monodisperse particles with no or limited aggregation. Due to the limited mass transfer observed when the reactions were performed in aqueous buffer solution (Table 1, entries 11–13) we attempted the reaction in 25% DMSO to aid the dissolution of substrates. The results showed a significant increase in the yield between 75 and 81%, for both citrate and phosphate, at pH 6 and 7 (entries 2–3 and 5–6), while maintaining good ee (up to 89%) and moderate diastereoselectivity (67:33). Aldol reactions are known to be responsive to pH changes [76]; therefore, the use of buffer can be efficient in influencing the reaction medium. When the reactions were carried out at a low pH of 5.8 (entries 1 and 7), the reactions proceeded slowly, with yields of 68 and 75%, respectively. The observed results were in agreement with what was previously reported [79]. Moderate selectivities and diastereoselectivity were also observed. The reactions were not favourable in Tris buffer, as yields (up to 53%) did not significantly improve and selectivities also decreased. The hypothesis for this buffer behaviour is unclear, but we do not exclude the possibility of the weak buffering capacity

of Tris buffer, which is around 7–9, potentially explaining the poor reaction. Control experiments revealed trace amounts of the product, as observed using TLC. There was no notable difference in the results obtained using either citrate or phosphate, and therefore further investigations were performed using phosphate buffer at pH 7. In comparison to citrate buffer, phosphate buffer displays poor colloidal stability of nanoparticles due to competing interactions of phosphate ions with Au ions which lead to quick aggregation [74]. The colloidal stability of gold nanoparticles in citrate buffer has been demonstrated by other research groups [46,80,81]. The peptide–AuNP-catalyzed aldol reaction was therefore investigated in citrate buffer (pH = 7), and the results are shown in Table 3.

Table 2. Effect of buffer and pH on peptide–AuNPs catalyzed aldol reaction between *p*-nitrobenzaldehyde and cyclohexanone [a].

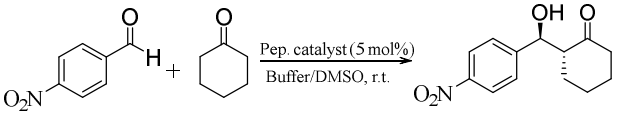

Entry	Buffer	pH	Time (h)	Yield [b]	ee(%) [c]	dr (Anti:Syn) [d]
1	Phosphate	5.6	72	70	69	67:30
2		6.5	72	78	86	64:36
3		7.0	72	81	89	62:38
4	Citrate	5.6	72	68	80	61:39
5		6.5	72	75	74	62:38
6		7.0	72	80	86	60:40
7	Tris	5.6	72	42	63	55:45
8		6.5	72	53	60	58:42
9		7.0	72	65	65	50:50
10	Control-Phosphate [e]	5.6	72	Trace	-	-
11		6.5	72	Trace	-	-
12		7.0	72	Trace	-	-
13	Control-citrate [e]	5.6	72	Trace	-	-
14		6.5	72	Trace	-	-
15		7.0	72	Trace	-	-
16	Control-Tris [e]	5.6	72	Trace	-	-
17		6.5	72	Trace	-	-
18		7.0	72	Trace	-	-

[a] The reaction was performed using *p*-nitrobenzaldehyde (0.157 mmol, 24 mg), cyclohexanone (0.628 mmol, 70 µL) and peptide catalyst (5 mol%) dissolved in 0.75 mL of a 3:1 50 mM buffer solution and DMSO, at room temperature. [b] Isolated yield. [c] ee values determined by chiral-phase HPLC analysis. [d] Determined by ^{1}H NMR analysis of the crude product. [e] The reaction was performed without a peptide–AuNPs catalyst.

Table 3. Aldol reaction catalyzed peptide–AuNPs in aqueous buffer solution [a].

Entry	Particle Size (nm)	Time (h)	Yield (%) [b]	ee (%) [c]	dr (Anti:Syn) [d]
1	16	48	77	88	62:38
2	15	48	81	79	49:51
3	12	48	85	74	47:53

[a] The reaction was performed using *p*-nitrobenzaldehyde (0.157 mmol, 24 mg), cyclohexanone (0.628 mmol, 70 µL) and peptide catalyst (6 mol%) dissolved in 0.75 mL of a 3:1 buffer solution and DMSO, at room temperature. [b] Isolated yield. [c] ee values determined by chiral-phase HPLC analysis. [d] Determined by ^{1}H NMR analysis of the crude product.

The results reveal a significant increase in the yield (up to 85%) (Table 3, entries 1–3), in comparison to the results presented in Table 1. The influence of the smaller particle size on catalytic activity is also demonstrated. As expected, the solution's pH still had a significant

influence on both the enantioselectivity and diastereoselectivity. The enhanced catalytic activity of enzyme-functionalized AuNPs is understood to be regulated by favourable conformational changes [72,82,83]. Hence the increased catalytic activity was attributed to the influence of the buffer solution on the colloidal stability of the nanoparticles, which in turn influenced the mobility of the reactants as well as structural flexibility [5,47].

3. Structural Analyses of Peptide in Solution and Pep–AuNPs in Solution

In order to explore the structural changes of the peptide upon conjugation to AuNPs, CD (circular dichroism) experiments were performed. The experiments were recorded in both buffer and water to compare the difference in structural folding and conformation in these solutions. The results for the CD experiments are presented below in Figure 6.

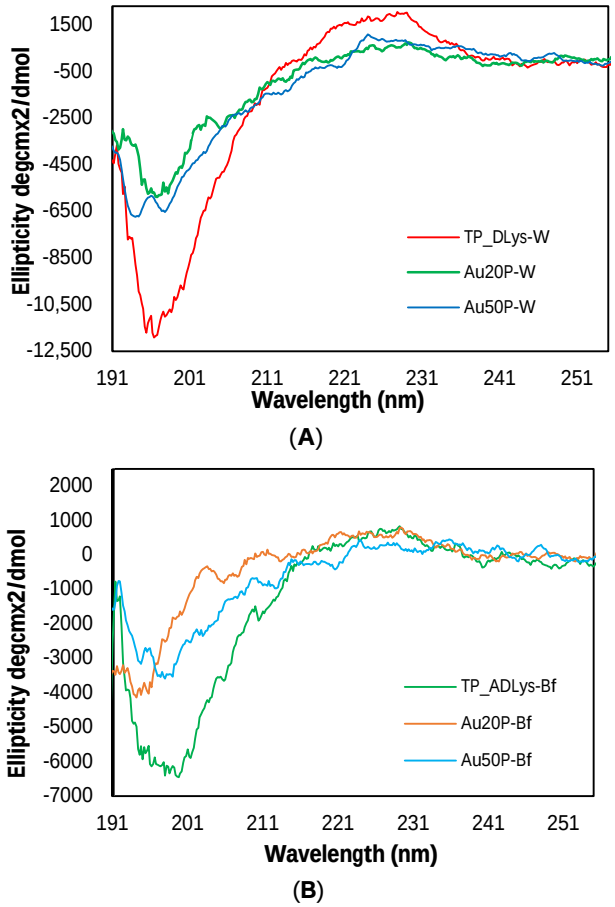

Figure 6. (**A**) Circular dichroism (CD) spectra in water for unbound peptide (TP_ADLys-W) and bounded peptide using 16 nm (Au20P-W) and 12 nm (Au50P-W) nanoparticles; (**B**) circular dichroism (CD) spectra in buffer for unbound peptide (TP_ADLys-Bf) and bounded peptide using 16 nm (Au20P-Bf) and 12 nm (Au50P-Bf) nanoparticles, respectively.

The CD data for the unbound peptide (TP_ADLys) in water reveal a single ellipticity minimum at 197 nm, which is characteristic of a random coil structure. For peptide-conjugated nanoparticles synthesized from both 12 and 16 nm particles, there is an observed trough with decreased ellipticity at 194 and 195 nm, respectively, and this was attributed to minor conformational changes caused by the affinity of the peptide to AuNPs [84]. The observed results further suggest that some fraction of the peptide molecules may not be bound to the Au surfaces; therefore, only minor conformational changes were observed, and this is similar to what was previously reported [21,47]. To further investigate the structural changes of the free and bound peptide, the CD experiments were performed in an aqueous buffer solution at pH 7.0, and the results are shown in Figure 6. As illustrated

in the figure, the CD profile in buffer solution for free peptide indicates that a large fraction of the peptide has no defined structure, with a broader negative band at 200 nm, which is a characteristic of a random coil. For the bound peptides, the CD spectra also show two minima bands with decreased ellipticity around 195 and 198 nm when the conjugates are synthesized from 16 and 12 nm nanoparticles, respectively, indicating possible affinity of the peptide to the AuNPs.

4. Conclusions

In summary, the first peptide–AuNP-catalyzed aldol reaction between cyclohexanone and *p*-nitrobenzaldehyde was successful. The pep–AuNP-catalyzed aldol reaction was demonstrated with moderate yields (up to 86%) and selectivity (up to 89%). The conjugation of AuNPs to peptide resulted in the increased conversion rate of the substrate, presumably due to the electron transfer rates [85]. Raman and XPS demonstrated the interaction of the peptide with gold nanoparticles. The use of a buffer solution resulted in colloidal stability, and therefore the catalytic activity of the pep–AuNPs was enhanced. This was attributed to the small conformational changes which facilitate the mobility of the reactants as well as the structural flexibility of the active site. The methodology described in this study presents the advantages of a novel and promising immobilized organocatalyst, which might be beneficial for other asymmetric reactions, and could also be applied to other systems. Further modifications to increase the scope of tolerance and improve the catalytic efficiency of the pep–AuNPs catalyst are under investigation, and studies involving mechanistic analyses of the peptide–AuNP conjugates will be reported soon.

The efficiency (yield = 15–85%; ee $\leq$ 94%) of the catalyst presented in this study is comparable to some catalysts reported in the literature, by Wennemer and coworkers (yield = 30–99%; ee $\leq$ 96%) [30], Wu et al. (yield = 3–97%; ee $\leq$ 99%) [86], Reiser and coworkers (yield = 36–98%; ee $\leq$ 95%) [69] and Alves et al. (yield = 7–62%; ee $\leq$ 86%) [87]. The Au-immobilized catalyst is a low-loading catalyst that produces aldol products with moderate yields and considerable enantioselectivity. While appreciating the outstanding advances in this field, we believe this work presents insight into the design of enzyme mimics and catalyst immobilization.

Supplementary Materials: The following supporting information can be downloaded at https://www.mdpi.com/article/10.3390/catal14110826/s1.

Author Contributions: M.M.M. was involved in the conceptualization of the work, and was also responsible for the administration, rewriting and revision of the manuscript. T.P. designed and performed the formal experiments, formal analysis of the data and wrote the manuscript. D.B. assisted with the interpretation of the results and writing (review and editing) of the manuscript. N.P.S. and K.M. assisted with the synthesis and characterisation of the AuNPs, N.M. was involved with the supervision, analysis and characterisation of the AuNPs. T.A. performed the CD experiments. All authors have read and agreed to the published version of the manuscript.

Funding: The authors are grateful to the DSI Industrial Biocatalysis Hub and the National Research Foundation (NRF), Thuthuka Award (Gun 117975) and CSUR (Grant No: 138081) for financial support.

Data Availability Statement: Data are contained within the article and Supplementary Materials.

Acknowledgments: The authors would like to express special thanks to the University of the Witwatersrand, the DSI/TIA Industrial Biocatalysis Hub and the National Research Foundation (NRF) for funding. The authors greatly acknowledge the Mass spectrometry division and microscopy and microanalysis unit at the University of the Witwatersrand.

Conflicts of Interest: The authors declare no competing financial interests.

Abbreviations

AuNPs, gold nanoparticles; NPs, nanoparticles; $HAuCl_4$, hydrogen tetrachlorocuprate; FBPA, fructose-1,6-bisphosphate aldolase enzyme; TEM, transmission electron microscopy; DMSO, dimethyl

sulfoxide; CD, circular dichroism; ee, enantiomeric excess; TLC, thin layer chromatography.

References

1. Melchiorre, P.; Marigo, M.; Carlone, A.; Bartoli, G. Asymmetric Aminocatalysis—Gold Rush in Organic Chemistry. *Angew. Chem.-Int. Ed.* **2008**, *47*, 6138–6171. [CrossRef] [PubMed]
2. Dalko, P.I.; Moisan, L. In the Golden Age of Organocatalysis. *Angew. Chem.-Int. Ed.* **2004**, *43*, 5138–5175. [CrossRef] [PubMed]
3. Alemán, J.; Cabrera, S. Applications of Asymmetric Organocatalysis in Medicinal Chemistry. *Chem. Soc. Rev.* **2013**, *42*, 774–793. [CrossRef] [PubMed]
4. Susam, Z.D.; Tanyeli, C. Recyclable Organocatalysts in Asymmetric Synthesis. *Asian J. Org. Chem.* **2021**, *10*, 1251–1266. [CrossRef]
5. Kumar, A.; Dewan, M.; De, A.; Saxena, A.; Aerry, S.; Mozumdar, S. Aldol Condensation in PEG-400 Catalyzed by Recyclable l-Proline Supported on Nano Gold Surface. *RSC Adv.* **2013**, *3*, 603–607. [CrossRef]
6. Malkov, A.V.; Figlus, M.; Cooke, G.; Caldwell, S.T.; Rabani, G.; Prestly, M.R.; Kočovský, P. Organocatalysts Immobilised onto Gold Nanoparticles: Application in the Asymmetric Reduction of Imines with Trichlorosilane. *Org. Biomol. Chem.* **2009**, *7*, 1878–1883. [CrossRef]
7. Rodríguez-Llansola, F.; Miravet, J.F.; Escuder, B. A Supramolecular Hydrogel as a Reusable Heterogeneous Catalyst for the Direct Aldol Reaction. *Chem. Commun.* **2009**, *10*, 7303–7305. [CrossRef]
8. Arakawa, Y.; Wiesner, M.; Wennemers, H. Efficient Recovery and Reuse of an Immobilized Peptidic Organocatalyst. *Adv. Synth. Catal.* **2011**, *353*, 1201–1206. [CrossRef]
9. Ayats, C.; Henseler, A.H.; Pericás, M.A. A Solid-Supported Organocatalyst for Continuous-Flow Enantioselective Aldol Reactions. *ChemSusChem* **2012**, *5*, 320–325. [CrossRef]
10. Kong, Y.; Tan, R.; Zhao, L.; Yin, D. L-Proline Supported on Ionic Liquid-Modified Magnetic Nanoparticles as a Highly Efficient and Reusable Organocatalyst for Direct Asymmetric Aldol Reaction in Water. *Green Chem.* **2013**, *15*, 2422–2433. [CrossRef]
11. Surujpaul, P.P.; Gutiérrez-wing, C.; Ocampo-garcía, B.; Ramírez, F.D.M.; De Murphy, C.A. Gold Nanoparticles Conjugated to [Tyr 3] Octreotide Peptide. *Biophys. Chem.* **2008**, *138*, 83–90. [CrossRef] [PubMed]
12. Ocampo-García, B.E.; de Ramírez, F.M.; Ferro-Flores, G.; De León-Rodríguez, L.M.; Santos-Cuevas, C.L.; Morales-Avila, E.; de Murphy, C.A.; Pedraza-López, M.; Medina, L.A.; Camacho-López, M.A. 99mTc-Labelled Gold Nanoparticles Capped with HYNIC-Peptide/Mannose for Sentinel Lymph Node Detection. *Nucl. Med. Biol.* **2011**, *38*, 1–11. [CrossRef] [PubMed]
13. Lee, K.H.; Marty Ytreberg, F. Effect of Gold Nanoparticle Conjugation on Peptide Dynamics and Structure. *Entropy* **2012**, *14*, 630–641. [CrossRef]
14. Porta, F.; Speranza, G.; Krpetić, Ž.; Dal Santo, V.; Francescato, P.; Scarì, G. Gold Nanoparticles Capped by Peptides. *Mater. Sci. Eng. B Solid-State Mater. Adv. Technol.* **2007**, *140*, 187–194. [CrossRef]
15. Liu, S.; Lämmerhofer, M. Functionalized Gold Nanoparticles for Sample Preparation: A Review. *Electrophoresis* **2019**, *40*, 2438–2461. [CrossRef]
16. Mocanu, A.; Cernica, I.; Tomoaia, G.; Bobos, L.D.; Horovitz, O.; Tomoaia-Cotisel, M. Self-Assembly Characteristics of Gold Nanoparticles in the Presence of Cysteine. *Colloids Surf. A Physicochem. Eng. Asp.* **2009**, *338*, 93–101. [CrossRef]
17. Chai, F.; Wang, C.; Wang, T.; Ma, Z.; Su, Z. L-Cysteine Functionalized Gold Nanoparticles for the Colorimetric Detection of Hg2+ Induced by Ultraviolet Light. *Nanotechnology* **2010**, *21*, 025501. [CrossRef]
18. Wang, Q.; Yang, Z.; Gao, Y.; Ge, W.; Wang, L.; Xu, B. Enzymatic Hydrogelation to Immobilize an Enzyme for High Activity and Stability. *Soft Matter* **2008**, *4*, 550–553. [CrossRef]
19. Ardao, I.; Comenge, J.; Benaiges, M.D.; Álvaro, G.; Puntes, V.F. Rational Nanoconjugation Improves Biocatalytic Performance of Enzymes: Aldol Addition Catalyzed by Immobilized Rhamnulose-1-Phosphate Aldolase. *Langmuir* **2012**, *28*, 6461–6467. [CrossRef]
20. Pengo, P.; Baltzer, L.; Pasquato, L.; Scrimin, P. Substrate Modulation of the Activity of an Artificial Nanoesterase Made of Peptide-Functionalized Gold Nanoparticles. *Angew. Chem.* **2007**, *119*, 404–408. [CrossRef]
21. Mikolajczak, D.J.; Koksch, B. Carbonic Anhydrase Mimics. *Catalysts* **2019**, *9*, 903. [CrossRef]
22. Storhoff, J.J.; Elghanian, R.; Mucic, R.C.; Mirkin, C.A.; Letsinger, R.L. One-Pot Colorimetric Differentiation of Polynucleotides with Single Base Imperfections Using Gold Nanoparticle Probes. *J. Am. Chem. Soc.* **1998**, *120*, 1959–1964. [CrossRef]
23. Slocik, J.M.; Zabinski, J.S.; Phillips, D.M.; Naik, R.R. Colorimetric Response of Peptide-Functionalized Gold Nanoparticles to Metal Ions. *Small* **2008**, *4*, 548–551. [CrossRef] [PubMed]
24. Shukla, R.; Hill, E.; Shi, X.; Kim, J.; Muniz, M.C.; Baker, J.R. Tumor Microvasculature Targeting with Dendrimer-Entrapped Gold Nanoparticles. *Soft Matter* **2008**, *4*, 2160–2163. [CrossRef]
25. Pengo, P.; Polizzi, S.; Pasquato, L.; Scrimin, P. Carboxylate-Imidazole Cooperativity in Dipeptide-Functionalized Gold Nanoparticles with Esterase-like Activity. *J. Am. Chem. Soc.* **2005**, *127*, 1616–1617. [CrossRef]
26. Mikolajczak, D.J.; Heier, J.L.; Schade, B.; Koksch, B. Catalytic Activity of Peptide-Nanoparticle Conjugates Regulated by a Conformational Change. *Biomacromolecules* **2017**, *18*, 3557–3562. [CrossRef]
27. Sóti, P.L.; Yamashita, H.; Sato, K.; Narumi, T.; Toda, M.; Watanabe, N.; Marosi, G.; Mase, N. Synthesis of a Self-Assembling Gold Nanoparticle-Supported Organocatalyst for Enamine-Based Asymmetric Aldol Reactions. *Tetrahedron* **2016**, *72*, 1984–1990. [CrossRef]

28. Khiar, N.; Navas, R.; Elhalem, E.; Valdivia, V.; Fernández, I. Proline-Coated Gold Nanoparticles as a Highly Efficient Nanocatalyst for the Enantioselective Direct Aldol Reaction in Water. *RSC Adv.* **2013**, *3*, 3861–3864. [CrossRef]
29. Akagawa, K.; Sakamoto, S.; Kudo, K. Direct Asymmetric Aldol Reaction in Aqueous Media Using Polymer-Supported Peptide. *Tetrahedron Lett.* **2005**, *46*, 8185–8187. [CrossRef]
30. Krattiger, P.; Kovasy, R.; Revell, J.D.; Ivan, S.; Wennemers, H. Increased Structural Complexity Leads to Higher Activity: Peptides as Efficient and Versatile Catalysts for Asymmetric Aldol Reactions. *Org. Lett.* **2005**, *7*, 1101–1103. [CrossRef]
31. Wennemers, H. Peptides as Asymmetric Catalysts and Templates for the Controlled Formation of Ag Nanoparticles. *J. Pept. Sci.* **2012**, *18*, 437–441. [CrossRef] [PubMed]
32. Huang, W.; Tian, H.; Xu, H.; Zheng, L.; Liu, Q.; Zhang, S. L-Valine Dipeptide Organocatalysts with Two Amide Units for the Direct Asymmetric Aldol Reaction in Brine. *Catal. Lett.* **2011**, *141*, 872–876. [CrossRef]
33. Szollosi, G.; Csámpai, A.; Somlai, C.; Fekete, M.; Bartók, M. Unusual Enantioselectivities in Heterogeneous Organocatalyzed Reactions: Reversal of Direction Using Proline Di- versus Tri-Peptides in the Aldol Addition. *J. Mol. Catal. A Chem.* **2014**, *382*, 86–92. [CrossRef]
34. Aili, D.; Stevens, M.M. Bioresponsive Peptide–Inorganic Hybrid Nanomaterials. *Chem. Soc. Rev.* **2010**, *39*, 3528–3540. [CrossRef]
35. Peme, T.; Brady, D.; Juma, W.; Makatini, M. Development of Fructose-1,6-Bisphosphate Aldolase Enzyme Peptide Mimics as Biocatalysts in Direct Asymmetric Aldol Reactions. *RSC Adv.* **2021**, *11*, 36670–36681. [CrossRef]
36. Lévy, R.; Thanh, N.T.K.; Christopher Doty, R.; Hussain, I.; Nichols, R.J.; Schiffrin, D.J.; Brust, M.; Fernig, D.G. Rational and Combinatorial Design of Peptide Capping Ligands for Gold Nanoparticles. *J. Am. Chem. Soc.* **2004**, *126*, 10076–10084. [CrossRef]
37. Pale-Grosdemange, C.; Simon, E.S.; Prime, K.L.; Whitesides, G.M. Formation of Self-Assembled Monolayers by Chemisorption of Derivatives of Oligo(Ethylene Glycol) of Structure HS(CH2)11(OCH2CH2)MOH on Gold. *J. Am. Chem. Soc.* **1991**, *113*, 12–20. [CrossRef]
38. Tullman, J.A.; Finney, W.F.; Lin, Y.J.; Bishnoi, S.W. Tunable Assembly of Peptide-Coated Gold Nanoparticles. *Plasmonics* **2007**, *2*, 119–127. [CrossRef]
39. Dahl, J.A.; Maddux, B.L.S.; Hutchison, J.E.; Dahl, J.A.; Maddux, B.L.S.; Hutchison, J.E. Toward Greener Nanosynthesis. *Chem. Rev.* **2007**, *107*, 2228–2269. [CrossRef]
40. Natarajan, P.; Sukthankar, P.; Changstrom, J.; Holland, C.S.; Barry, S.; Hunter, W.B.; Sorensen, C.M.; Tomich, J.M. Synthesis and Characterization of Multifunctional Branched Amphiphilic Peptide Bilayer Conjugated Gold Nanoparticles. *ACS Omega* **2018**, *3*, 11071–11083. [CrossRef]
41. Jia, Y.; Yan, X.; Guo, X.; Zhou, G.; Liu, P.; Li, Z. One Step Preparation of Peptide-Coated Gold Nanoparticles with Tunable Size. *Materials* **2019**, *12*, 2107. [CrossRef] [PubMed]
42. Castro-Longoria, E.; Vilchis-Nestor, A.R.; Avalos-Borja, M. Biosynthesis of Silver, Gold and Bimetallic Nanoparticles Using the Filamentous Fungus Neurospora Crassa. *Colloids Surf. B Biointerfaces* **2011**, *83*, 42–48. [CrossRef] [PubMed]
43. Martinsson, E.; Sepulveda, B.; Chen, P.; Elfwing, A.; Liedberg, B.; Aili, D. Optimizing the Refractive Index Sensitivity of Plasmonically Coupled Gold Nanoparticles. *Plasmonics* **2014**, *9*, 773–780. [CrossRef]
44. Chen, C.F.; Tzeng, S.D.; Chen, H.Y.; Lin, K.J.; Gwo, S. Tunable Plasmonic Response from Alkanethiolate-Stabilized Gold Nanoparticle Superlattices: Evidence of near-Field Coupling. *J. Am. Chem. Soc.* **2008**, *130*, 824–826. [CrossRef]
45. Zong, J.; Cobb, S.L.; Cameron, N.R. Peptide-Functionalized Gold Nanoparticles: Versatile Biomaterials for Diagnostic and Therapeutic Applications. *Biomater. Sci.* **2017**, *5*, 872–886. [CrossRef]
46. Aili, D.; Enander, K.; Rydberg, J.; Lundström, I.; Baltzer, L.; Liedberg, B. Aggregation-Induced Folding of a de Novo Designed Polypeptide Immobilized on Gold Nanoparticles. *J. Am. Chem. Soc.* **2006**, *128*, 2194–2195. [CrossRef]
47. Aili, D.; Enander, K.; Rydberg, J.; Nesterenko, I.; Björefors, F.; Baltzer, L.; Liedberg, B. Folding Induced Assembly of Polypeptide Decorated Gold Nanoparticles. *J. Am. Chem. Soc.* **2008**, *130*, 5780–5788. [CrossRef]
48. Schneider, C.A.; Rasband, W.S.; Eliceiri, K.W. NIH Image to ImageJ: 25 Years of Image Analysis HHS Public Access. *Nat. Methods* **2012**, *9*, 671–675. [CrossRef]
49. Mlambo, M.; Harris, R.A.; Mashazi, P.; Sabela, M.; Kanchi, S.; Madikizela, L.M.; Shumbula, P.N.; Moloto, N.; Hlatshwayo, T.T.; Mdluli, P.S. Computational and Experimental Evaluation of Selective Substitution of Thiolated Coumarin Derivatives on Gold Nanoparticles: Surface Enhancing Raman Scattering and Electrochemical Studies. *Appl. Surf. Sci.* **2017**, *396*, 695–704. [CrossRef]
50. Chow, M.K.; Zukoski, C.F. Gold Sol Formation Mechanisms: Role of Colloidal Stability. *J. Colloid Interface Sci.* **1994**, *165*, 97–109. [CrossRef]
51. Tran, M.; DePenning, R.; Turner, M.; Padalkar, S. Effect of Citrate Ratio and Temperature on Gold Nanoparticle Size and Morphology. *Mater. Res. Express* **2016**, *3*, 105027. [CrossRef]
52. Turkevich, J.; Stevenson, P.C.; Hillier, J. A Study of the Nucleation and Growth Processes in the Synthesis of Colloidal Gold. *Discuss. Faraday Soc.* **1951**, *11*, 55–75. [CrossRef]
53. Wang, S.; Qian, K.; Bi, X.; Huang, W. Influence of Speciation of Aqueous HAuCl4 on the Synthesis, Structure, and Property of Au Colloids. *J. Phys. Chem. C* **2009**, *113*, 6505–6510. [CrossRef]
54. Puddu, V.; Perry, C.C. Interactions at the Silica-Peptide Interface: The Influence of Particle Size and Surface Functionality. *Langmuir* **2014**, *30*, 227–233. [CrossRef] [PubMed]

55. Celentano, M.; Jakhmola, A.; Profeta, M.; Battista, E.; Guarnieri, D.; Gentile, F.; Netti, P.A.; Vecchione, R. Diffusion Limited Green Synthesis of Ultra-Small Gold Nanoparticles at Room Temperature. *Colloids Surf. A Physicochem. Eng. Asp.* **2018**, *558*, 548–557. [CrossRef]
56. Chenakin, S.P.; Kruse, N. Au 4f spin–orbit coupling effects in supported gold nanoparticles. *Phys. Chem. Chem. Phys.* **2016**, *18*, 22778–22782. [CrossRef]
57. Yah, C.S. The toxicity of Gold Nanoparticles in relation to their physiochemicalproperties. *Biomed. Res.* **2013**, *24*, 400–413.
58. Casaletto, M.P.; Longo, A.; Martorana, A.; Prestianni, A.; Venezia, A.M. XPS study of supported gold catalysts: The role of Au^0 and $Au^{+\delta}$ species as active sites. *Surf. Interface. Anal.* **2006**, *38*, 215–218. [CrossRef]
59. Tran, N.T.T.; Wang, T.-H.; Lin, C.-Y.; Tsai, Y.-C.; Lai, C.-H.; Tai, Y.; Yung, B.Y.M. Direct Synthesis of Rev Peptide-Conjugated Gold Nanoparticles and Their Application in Cancer Therapeutics. *Bioconjug. Chem.* **2011**, *22*, 1394–1401. [CrossRef]
60. Ahmad, F.; Salem-Bekhit, M.M.; Khan, F.; Alshehri, S.; Khan, A.; Ghoneim, M.M.; Wu, H.-F.; Taha, E.I.; Elbagory, I. Unique Properties of Surface-Functionalized Nanoparticles for Bio-Application: Functionalization Mechanisms and Importance in Application. *Nanomaterials* **2022**, *12*, 1333. [CrossRef]
61. Rana, A.; Yadav, K.; Jagadevan, S. A comprehensive review on green synthesis of nature-inspired metal nanoparticles: Mechanism, application and toxicity. *J Clean. Prod.* **2020**, *272*, 122880. [CrossRef]
62. Jin, Z.; Yeung, J.; Zhou, J.; Retout, M.; Yim, W.; Fajtová, P.; Gosselin, B.; Jabin, I.; Bruylants, G.; Mattoussi, H.; et al. Empirical Optimization of Peptide Sequence and Nanoparticle Colloidal Stability: The Impact of Surface Ligands and Implications for Colorimetric Sensing. *ACS Appl. Mater. Interfaces* **2023**, *15*, 20483–20494. [CrossRef] [PubMed]
63. Pilot, R.; Signorini, R.; Durante, C.; Orian, L.; Bhamidipati, M.; Fabris, L. A Review on Surface-Enhanced Raman Scattering. *Biosensors* **2019**, *9*, 52. [CrossRef]
64. Liu, X.; Zhang, Q.; Knoll, W.; Liedberg, B.; Wang, Y. Rational Design of Functional Peptide–Gold Hybrid Nanomaterials for Molecular Interactions. *Adv. Mater.* **2020**, *32*, 1–37. [CrossRef]
65. Jiang, Z.; Yang, H.; Han, X.; Luo, J.; Wong, M.W.; Lu, Y. Direct Asymmetric Aldol Reactions between Aldehydes and Ketones Catalyzed by L-Tryptophan in the Presence of Water. *Org. Biomol. Chem.* **2010**, *8*, 1368–1377. [CrossRef]
66. Li, W.; Liu, D.; Geng, X.; Li, Z.; Gao, R. Real-Time Regulation of Catalysis by Remote-Controlled Enzyme-Conjugated Gold Nanorod Composites for Aldol Reaction-Based Applications. *Catal. Sci. Technol.* **2019**, *9*, 2221–2230. [CrossRef]
67. Lei, M.; Shi, L.; Li, G.; Chen, S.; Fang, W.; Ge, Z.; Cheng, T.; Li, R. Dipeptide-Catalyzed Direct Asymmetric Aldol Reactions in the Presence of Water. *Tetrahedron* **2007**, *63*, 7892–7898. [CrossRef]
68. Knowles, R.R.; Jacobsen, E.N. Attractive Noncovalent Interactions in Asymmetric Catalysis: Links between Enzymes and Small Molecule Catalysts. *Proc. Natl. Acad. Sci. USA* **2010**, *107*, 20678–20685. [CrossRef]
69. D'Elia, V.; Zwicknagl, H.; Reiser, O. Short α/β-Peptides as Catalysts for Intra- and Intermolecular Aldol Reactions. *J. Org. Chem.* **2008**, *73*, 3262–3265. [CrossRef]
70. Córdova, A.; Zou, W.; Dziedzic, P.; Ibrahem, I.; Reyes, E.; Xu, Y. Direct Asymmetric Intermolecular Aldol Reactions Catalyzed by Amino Acids and Small Peptides. *Chem.—Eur. J.* **2006**, *12*, 5383–5397. [CrossRef]
71. Lin, J.H.; Zhang, C.P.; Xiao, J.C. Enantioselective Aldol Reaction of Cyclic Ketones with Aryl Aldehydes Catalyzed by a Cyclohexanediamine Derived Salt in the Presence of Water. *Green Chem.* **2009**, *11*, 1750–1753. [CrossRef]
72. Wu, C.S.; Wu, C.T.; Yang, Y.S.; Ko, F.H. An Enzymatic Kinetics Investigation into the Significantly Enhanced Activity of Functionalized Gold Nanoparticles. *Chem. Commun.* **2008**, *42*, 5327–5329. [CrossRef] [PubMed]
73. Pallares, R.M.; Stilson, T.; Choo, P.; Hu, J.; Odom, T.W. Using Good's Buffers to Control the Anisotropic Structure and Optical Properties of Spiky Gold Nanoparticles for Refractive Index Sensing. *ACS Appl. Nano Mater.* **2019**, *2*, 5266–5271. [CrossRef]
74. Sangwan, S.; Seth, R. Synthesis, Characterization and Stability of Gold Nanoparticles (AuNPs) in Different Buffer Systems. *J. Clust. Sci.* **2022**, *33*, 749–764. [CrossRef]
75. Barreto, Â.; Luis, L.G.; Girão, A.V.; Trindade, T.; Soares, A.M.V.M.; Oliveira, M. Behavior of Colloidal Gold Nanoparticles in Different Ionic Strength Media. *J. Nanopart. Res.* **2015**, *17*, 1–13. [CrossRef]
76. Birolli, W.G.; Fonseca, L.P.; Porto, A.L.M. Aldol Reactions by Lipase From Rhizopus Niveus, an Example of Unspecific Protein Catalysis. *Catal. Lett.* **2017**, *147*, 1977–1987. [CrossRef]
77. Harrison, E.; Hamilton, J.W.J.; Macias-Montero, M.; Dixon, D. Peptide Functionalized Gold Nanoparticles: The Influence of PH on Binding Efficiency. *Nanotechnology* **2017**, *28*, 295602. [CrossRef]
78. Xie, Z.B.; Wang, N.; Jiang, G.F.; Yu, X.Q. Biocatalytic Asymmetric Aldol Reaction in Buffer Solution. *Tetrahedron Lett.* **2013**, *54*, 945–948. [CrossRef]
79. Dziedzic, P.; Zou, W.; Háfren, J.; Córdova, A. The Small Peptide-Catalyzed Direct Asymmetric Aldol Reaction in Water. *Org. Biomol. Chem.* **2006**, *4*, 38–40. [CrossRef]
80. Ji, X.; Song, X.; Li, J.; Bai, Y.; Yang, W.; Peng, X. Size Control of Gold Nanocrystals in Citrate Reduction: The Third Role of Citrate. *J. Am. Chem. Soc.* **2007**, *129*, 13939–13948. [CrossRef]
81. Biggs, S.; Mulvaney, P.; Zukoski, C.F.; Grieser, F. Study of Anion Adsorption at the Gold-Aqueous Solution Interface by Atomic Force Microscopy. *J. Am. Chem. Soc.* **1994**, *116*, 9150–9157. [CrossRef]
82. Pandey, P.; Singh, S.P.; Arya, S.K.; Gupta, V.; Datta, M.; Singh, S.; Malhotra, B.D. Application of Thiolated Gold Nanoparticles for the Enhancement of Glucose Oxidase Activity. *Langmuir* **2007**, *23*, 3333–3337. [CrossRef] [PubMed]

83. Gole, A.; Dash, C.; Ramakrishnan, V.; Sainkar, S.R.; Mandale, A.B.; Rao, M.; Sastry, M. Pepsin-Gold Colloid Conjugates: Preparation, Characterization, and Enzymatic Activity. *Langmuir* **2001**, *17*, 1674–1679. [CrossRef]
84. Li, Y.; Tang, Z.; Prasad, P.N.; Knecht, M.R.; Swihart, M.T. Peptide-Mediated Synthesis of Gold Nanoparticles: Effects of Peptide Sequence and Nature of Binding on Physicochemical Properties. *Nanoscale* **2014**, *6*, 3165–3172. [CrossRef]
85. Park, J.; Joo, J.; Soon, G.K.; Jang, Y.; Hyeon, T. Synthesis of Monodisperse Spherical Nanocrystals. *Angew. Chem.-Int. Ed.* **2007**, *46*, 4630–4660. [CrossRef]
86. Zhang, N.; Sun, Z.; Wu, C. Artificial Enzymes Combining Proteins with Proline Polymers for Asymmetric Aldol Reactions in Water. *ACS Catal.* **2022**, *12*, 4777–4783. [CrossRef]
87. Pelin, J.N.B.D.; Gerbelli, B.B.; Soares, B.M.; Aguilar, A.M.; Alves, W.A. Amyloidogenic Model Peptides as Catalysts for Stereoselective Aldol Reactions. *Catal. Sci. Technol.* **2019**, *9*, 4304–4313. [CrossRef]